A new cobalt-free proton-blocking composite cathode La$_2$NiO$_{4+\delta}$−LaNi$_{0.6}$Fe$_{0.4}$O$_{3-\delta}$ for BaZr$_{0.1}$Ce$_{0.7}$Y$_{0.2}$O$_{3-\delta}$-based solid oxide fuel cells

CrossMark

Jie Hou [a], Zhiwen Zhu [b], Jing Qian [a], Wei Liu [a,c,*]

[a] CAS Key Laboratory of Materials for Energy Conversion & Collaborative Innovation Center of Suzhou Nano Science and Technology, University of Science and Technology of China, Hefei 230026, PR China
[b] Institute of Urban Environment, Chinese Academy of Sciences, Xiamen 361021, PR China
[c] Key Laboratory of Materials Physics, Institute of Solid State Physics, Chinese Academy of Sciences, Hefei 230031, PR China

HIGHLIGHTS

- Series of LNO−LNF composites were firstly evaluated as cathodes for H-SOFC.
- The electrical conductivity of LNO−LNF73 reaches 99.2 S cm^{-1} at 650 °C.
- LNO−LNF73 is the most optimized combination among all composite cathodes.
- At 700 °C, the cell with LNO−LNF73 showed the highest MPD of 590 mW cm^{-2}.

ARTICLE INFO

ABSTRACT

Series of proton-blocking La$_2$NiO$_{4+\delta}$ (LNO)−LaNi$_{0.6}$Fe$_{0.4}$O$_{3-\delta}$ (LNF) (1:0, 7:3, 5:5, 3:7, 0:1 wt.%) composites were evaluated as cathodes for BaZr$_{0.1}$Ce$_{0.7}$Y$_{0.2}$O$_{3-\delta}$ (BZCY)-based proton-conducting solid oxide fuel cell (H-SOFC). The X-ray diffraction (XRD) results show a good chemical compatibility for each composition below 1100 °C. Electrochemical studies reveal that LNO−LNF73 shows the lowest area specific polarization resistance in symmetrical cells and the best electrochemical performance in single cell tests with the highest maximum power density (MPD) and the lowest interfacial polarization resistance (R_{p}). These results corroborate the electrical conductivity analysis. The single cell with LNO−LNF73 as cathode outputs the MPD of 590 mW cm^{-2} and the R_{p} of 0.091 Ω cm^2 at 700 °C. This work confirms that LNO−LNF73 composite material could be a promising cathode for H-SOFC.

© 2014 Elsevier B.V. All rights reserved.

1. Introduction

Solid oxide fuel cells (SOFCs) as a new power generation device has attracted worldwide attention since it provides many advantages over traditional energy conversion systems including high power conversion efficiency, excellent fuel adaptability, reliability, low pollutant levels, long operating life and so on [1−4]. Solid oxide proton conductors display lower activation energy than conventional oxygen-ion conductors such as YSZ and rare-earth doped ceria (DCO), and this would facilitate SOFCs based on proton-conducting electrolytes to have potential for higher proton conductivity and faster surface reactions at intermediate temperature of 400−700 °C [5−10]. The state-of-the-art proton conducting materials are BaCeO$_3$-based oxides. In particular, BaZr$_{0.1}$Ce$_{0.7}$Y$_{0.2}$O$_{3-\delta}$ (BZCY), which has been demonstrated to exhibit not only adequate proton conductivity but also sufficient chemical stability, is one of the most popular proton conductors [11,12].

It is generally recognized that the cathode is critical for the performance of SOFC [13−15]. An ideal SOFC cathode should have high catalytic activity, adequate electronic conductivity (100 S cm^{-1}), good thermal and chemical compatibility with the electrolyte and high chemical stability under desired operating conditions [1,16]. To increase the catalytic activity, the element cobalt is usually introduced into the cathode materials. A series of cobalt-containing mixed ionic and electronic conductors (MIECs)

* Corresponding author. CAS Key Laboratory of Materials for Energy Conversion & Collaborative Innovation Center of Suzhou Nano Science and Technology, University of Science and Technology of China, Hefei 230026, PR China. Tel.: +86 551 63606929; fax: +86 551 63602586.
E-mail address: wliu@ustc.edu.cn (W. Liu).

with simple perovskite structure, e.g. $Sm_{0.5}Sr_{0.5}CoO_{3-\delta}$ [14,17], $Ba_{0.6}Sr_{0.4}Co_{0.8}Fe_{0.2}O_{3-\delta}$ [18], $La_{0.6}Sr_{0.4}Co_{0.8}Fe_{0.2}O_{3-\delta}$ [19], $La_{0.5}Sr_{0.5}CoO_{3-\delta}$ [20] and $BaZr_{0.2}Co_{0.4}Fe_{0.4}O_{3-\delta}$ [21] or a layered perovskite structure, e.g. $SmBaCuCoO_{5+\delta}$ [22] and $LnBaCo_2O_{5+\delta}$ (Ln = Pr, Nd, Sm, Gd, Y) [23] have been extensively investigated as possible cathodes for H-SOFCs. However, cobalt-containing perovskite oxides often suffer problems like high thermal expansion coefficients (TEC), easy reduction, evaporation of cobalt and the high cost of cobalt element, thus limiting further applications [16,24]. Clearly, it would be significant to develop cobalt-free cathode materials with sufficient catalytic activity for H-SOFCs.

Recently, another family of MIECs referring to La_2NiO_4-based phases with K_2NiF_4-type structure have been studied as alternatives [25–27]. $La_2NiO_{4+\delta}$ (LNO) has the advantages of exhibiting relatively high oxygen diffusion ($D = 2 \times 10^{-7}$ cm^2 s^{-1}) and surface exchange coefficients ($k = 2 \times 10^{-6}$ cm s^{-1}) [28], as well as compatible TEC (13.0×10^{-6} K^{-1}) [29] with solid electrolytes and oxygen over-stoichiometry enabling the transportation of oxygen ions [30]. The crystal structure of LNO is formed by stacking alternate $LaNiO_3$ perovskite layers and La_2O_2 rocksalt layers along the c direction [31]. Significant excess oxygen, denoted as δ, can be incorporated into the La_2O_2 layers to decrease the structural stresses between the La–O and Ni–O bonding. At the same time, electron holes on nickel cations are created to satisfy the electroneutrality conservation while oxygen as interstitial defects in the rocksalt layers [32]. In the LNO-based materials, oxygen transport occurs via a complex mechanism combining interstitial migration in the rock-salt layers and vacancy migration in the perovskite planes. It has been demonstrated that the interstitial mechanism makes the main contribution to the oxygen ionic transport [33]. Therefore, the more oxygen overstoichiometry is achieved in these materials, the higher ionic conductivity can be expected. However, the low electronic conductivity (76 S cm^{-1} at 800 °C) [34] for the LNO material limits its practical application as an SOFC cathode. In contrast, rhombohedral phase $LaNi_{0.6}Fe_{0.4}O_{3-\delta}$ (LNF) used as SOFC cathode has certain advantages, including high electrical conductivity (580 S cm^{-1} at 800 °C) [35], a desirable TEC (average 11.4×10^{-6} K^{-1} from 30 to 1000 °C) [36], high electrochemical activity for the oxygen reduction reaction and excellent durability as regards chromium poisoning [37]. Considering the properties of these two different cathode materials, the composite cathode devised by mixing LNO with LNF (LNO–LNF) seems to be an optimal solution.

Sun et al. [11] firstly proposed the standpoint of proton-blocking composite cathode for H-SOFC. In proton-blocking composite cathode $La_{0.7}Sr_{0.3}FeO_{3-\delta}$–$Ce_{0.8}Sm_{0.2}O_{2-\delta}$ (LSF-SDC), dissociated oxygen ions transfer along the surface of the cathode or through the bulk of the cathode to triple phase boundaries (TPBs), and hence the electrochemical reactions mainly occur at the cathode–electrolyte interface [11,38]. As water is generated in cathode during operation for H-SOFC, when substituted SDC with BZCY, LSF–BZCY will adsorb more by-product water for the superior hydration behavior of BZCY. The water vapor partial pressure will be more higher, which will dilute the oxidant (air or oxygen) more severely in cathode layer. Meanwhile, the water occupies the cathode electrochemical reaction sites, which will weaken the cathode electrocatalytic ability. That is to say, water generating in cathode seems to be more detrimental for the performance of LSF–BZCY. Thus, although proton-blocking composite cathode LSF–SDC has less TPB or electrochemical reaction sites compared to proton-conducting composite cathode LSF–BZCY, it will be still able to exhibit a higher electro-catalytic ability which was validated by Sun et al. [11]. However, different from LSF–SDC, the oxygen ions transport in LNO–LNF composite is mainly through interstitial mechanism and there are no reports for this material as proton-blocking

composite cathode in H-SOFC. So given the above considerations, new cobalt-free proton-blocking $La_2NiO_{4+\delta}$–$LaNi_{0.6}Fe_{0.4}O_{3-\delta}$ (LNO–LNF) composites were firstly evaluated as cathodes for BZCY-based H-SOFC in this work. The chemical compatibility, electrical conductivity, microstructures and electrochemical performance with different ratio of LNO and LNF as cathodes were studied in detail.

2. Experimental

2.1. Preparation of powders

LNO, LNF and BZCY powders were synthesized via a citric acid–nitrate gel combustion process [14]. The raw materials for synthesis of LNO powders were La_2O_3, $Ni(NO_3)_2 \cdot H_2O$ and La_2O_3, $Ni(NO_3)_2 \cdot H_2O$ and $Fe(NO_3)_3 \cdot 9H_2O$ were used for synthesize LNF. $BaCO_3$, $Zr(NO_3)_4 \cdot 5H_2O$, $Ce(NO_3)_3 \cdot 6H_2O$ and $Y(NO_3)_3 \cdot 6H_2O$ served as the raw materials for BZCY powders. After the combustion, the all as-prepared ash-like powders were calcined at 1000 °C for 3 h in air to obtain LNO, LNF and BZCY powders, respectively.

2.2. Fabrication of symmetric cells and anode-supported single cells

The BZCY substrates for symmetric cells were fabricated with BZCY powders via die-pressing and then sintering at 1500 °C for 5 h in air. The average thickness and diameter of the sintered BZCY disks were approximately 1.0 and 12 mm, respectively.

The NiO–BZCY composite powders with a weight ratio of 6:4 for the anode substrates were prepared by the one-step gel combustion process [14]. The composite powders were calcined at 1000 °C for 3 h and then 20 wt.% starch was added as pore-creating materials to form sufficient porosity in the anode. The anode supported half cells were fabricated by a co-pressing method [39] and then co-fired at 1400 °C for 5 h.

LNO and LNF powders with weight ratio of 1:0, 7:3, 5:5, 3:7 and 0:1 were mixed thoroughly together with a 6 wt.% ethylcellulose–terpineol binder, to prepare five different cathode slurrys (LNO, LNO–LNF73, LNO–LNF55, LNO–NF37 and LNF). The slurrys were then painted onto the dense BZCY electrolyte disks or membranes and fired at 1000 °C for 3 h in air to form porous cathode layers. The effective area of the cathode layer in single cells was 0.237 cm^2.

2.3. Characterization and electrochemical measurements

Phase compositions of mixed powders contain LNO and LNF fired at various temperatures were identified by an X-ray diffractometer (Rigaku TTR-III) using CuKα radiation. The microstructures of the cell components were investigated by a scanning electron microscopy (SEM, JEOL JSM-6700F).

Five specimen bars with 40 mm × 5 mm × 2 mm dimension for the electrical conductivity measurements were prepared by pressing corresponding dry-mixed powders at 200 MPa. And then LNO and LNF bars sintered at 1400 °C for 5 h while LNO–LNF73, LNO–LNF55 and LNO–LNF37 sintered at 1100 °C for 20 h. The electrical conductivity was measured by a dc four-probe method from 200 to 800 °C at 50 °C intervals in air, and Ag paste was used for the electrodes. The conductivities (σ) were determined by taking $\sigma = L/A \times dI/dV$, where L is the distance between voltage contacts and A is the sample cross section.

All the single cells were tested in a home-made cell testing system at a temperature range of 550–700 °C under the same conditions for comparison. Humidified hydrogen (~3% H_2O) at a flow rate of 30 ml min^{-1} and ambient air were used as the fuel and the oxidant, respectively. The water vapor pressure about 0.03 atm was achieved by bubbling H_2 through water at about 25 °C. Ag paste
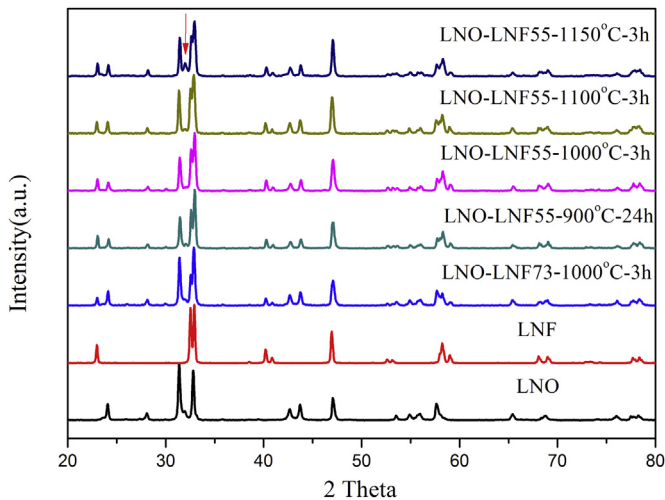
Fig. 1. XRD patterns of LNO–LNF73 fired at 1000 °C for 3 h and LNO–LNF55 fired from 900 to 1150 °C.

was applied to the cathode as a current collector and Ag wire was employed as the conducting wire. *I–V* curves of the cells were collected with a DC Electronic Load (ITech Electronics model IT8511) based on the two-probe configuration. The electrochemical impedance spectra were measured under open circuit conditions using an impedance analyzer (CHI604B, Shanghai Chenhua). A 5 mV a.c. signal was applied and the frequency was swept from 100 kHz to 0.1 Hz. The spectrum curve fitting was performed using the ZSimpWin Software. The equivalent circuit used to fit the plots was made of a resistance (*R*) and an inductance (*L*) associated in series with two distributed elements, composed by a constant phase element (CPE) in parallel with a resistance. Ohmic resistance and polarization resistance of the cells under open circuit conditions were estimated from the impedance spectra.

Symmetric cells applied for the impedance research was measured with an impedance analyzer (CHI604B, Shanghai Chenhua) (0.1–100 kHz, 5 mV as AC amplitude) which is same with the single cell test from 550 to 700 °C.

3. Results and discussion

3.1. Chemical stability

For composite cathodes LNO–LNF, the chemical compatibility between the MIEC LNO and the electrical conductor LNF at elevated temperatures should be firstly taken into account, since the solid state reaction between the two phases might generate less catalytic or non-conductive phases, which would lead to the

deterioration of the electrochemical activity of the cathode for oxygen reduction and charge transfer, and hence reduce cell performances.

Fig. 1 shows the XRD patterns of LNO–LNF73 fired at 1000 °C for 3 h and LNO–LNF55 fired from 900 to 1150 °C. It reveals that only typical peaks corresponding to LNO and LNF appear in the patterns, and no secondary phases can be identified below 1100 °C. When the firing temperature raised from 900 to 1000 °C, characteristic peaks of LNO–LNF compound has no significant deviation, owing to the as-prepared LNO and LNF powders calcined in 1000 °C for 3 h. And characteristic peaks of compound almost not shift with increasing firing temperature to 1100 °C, revealing a good chemical compatibility between the two compositions. However, when the firing temperature was up to 1150 °C, a small peak appeared that indicating the weak reaction. Anyhow, no undesirable insulating phases below 1100 °C are produced according to the XRD results. Besides, the cell parameters of LNO and LNF in LNO–LNF composites and single phase LNO and LNF powders calculated from XRD patterns were summarized in Table 1. Obviously, when the firing temperature was less than 1100 °C, no matter LNO–LNF73 or LNO–LNF55, the unit cell volume of LNO and LNF in composite has small variation. It indicates that the composites have negligible inter-diffusion of elements between LNO phase and LNF phase below 1100 °C. Therefore, we can conclude that LNO–LNF composite fired at 1000 °C doesn't influence the intrinsic electro-chemical catalytic activity of the composite material and this temperature could be an optimal temperature for preparing the cathode layer for H-SOFC.

3.2. Electrical conductivity

As LNO–LNF composites sintered at 1100 °C were not dense, the theoretical electrical conductivity of porous ceramics was calculated from the equation [40]:

$$\sigma = \sigma_0(1 - P)^\alpha \tag{1}$$

where, σ is the electrical conductivity of porous ceramics, σ_0 is the theoretical electrical conductivity of dense ceramics and P is the porosity. For regular shape geometry, α is a constant ($\alpha = 3.08 \pm 0.01$). The relative density (D) and the porosity (P) of the ceramics were obtained by the Archimedes method. The relative density of LNO, LNO–LNF73, LNO–LNF55, LNO–LNF37 and LNF specimens are 98.88%, 72.66%, 68.64%, 67.28% and 97.22%, while the corresponding porosity are 1.17%, 27.34%, 31.36%, 32.72% and 2.78%. For three kind composites, with adding more LNF, the relative density is lower. This phenomenon can be attributed to the better sintering activity of LNO compared with LNF. Fig. 2(a) shows the electrical conductivity of all specimens contain as a function of measuring temperature, respectively. In Fig. 2(a), the LNO and LNF show their real electrical conductivity while the

Table 1
Cell parameters of LNO and LNF in LNO–LNF composites and single phase LNO and LNF powders.

	LNO phase cell parameters			LNF phase cell parameters		
	a (Å)	*c* (Å)	*V* (Å³)	*a* (Å)	*c* (Å)	*V* (Å³)
LNO	3.843(1)	12.6329(8)	188.64(7)	—	—	—
LNF	—	—	—	5.5044(1)	13.2498(1)	347.66(1)
LNO–LNF73-3 h	3.8555(2)	12.6961(3)	188.72(3)	5.4967(4)	13.2713(5)	347.25(5)
LNO–LNF900-24 h	3.8576(3)	12.6708(8)	188.55(5)	5.4973(1)	13.2387(2)	346.47(3)
LNO–LNF900-3 h	3.8528(3)	12.6703(2)	188.08(2)	5.4977(1)	13.2397(2)	346.54(3)
LNO–LNF1000-3 h	3.8533(1)	12.6717(3)	188.15(3)	5.4914(5)	13.2495(8)	346.01(14)
LNO–LNF1100-3 h	3.8592(1)	12.6944(2)	189.05(2)	5.5095(1)	13.2275(2)	347.72(3)

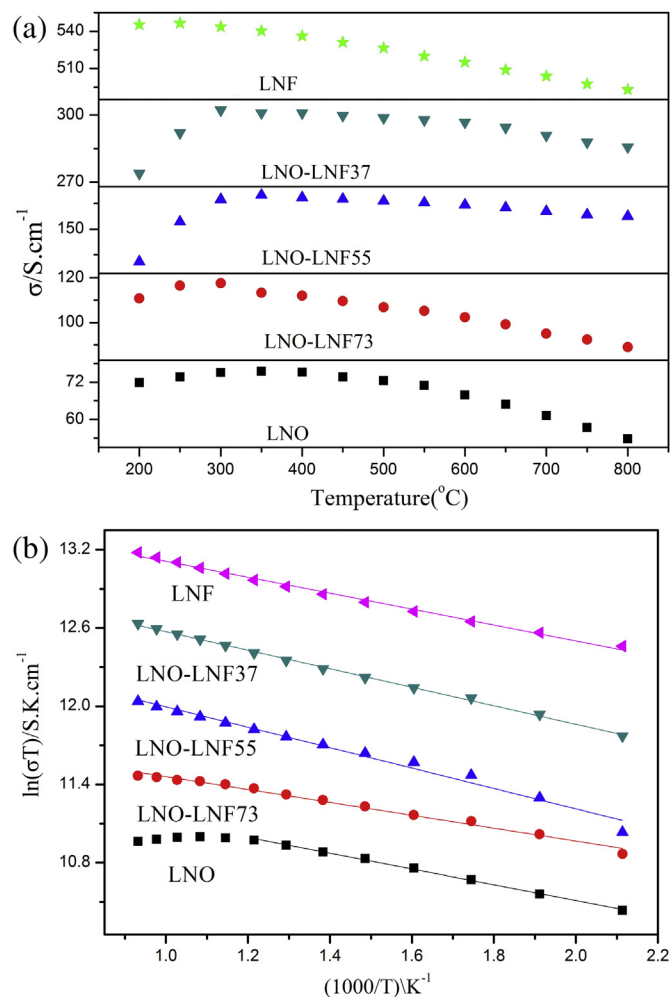LNF phase cell parameters are presented in hexagonal setting.

Fig. 2. (a) Electrical conductivity of all specimens contain as a function of measuring temperature, (b) and corresponding Arrhenius plots.

composites show the theoretical electrical conductivity. As it can be seen, the electrical conductivity of LNO, LNO–LNF73, LNO–LNF55 and LNO–LNF37 increase with measuring temperature up to a maximum value and then decrease, which undergoes a semiconducting-like conduction behavior to metal-like conduction behavior [41,42]. However, LNF almost decreases in measuring temperature range, which displays a metal-like conduction behavior. Compared with the pure LNF, the electrical conductivity values of LNO–LNF compositions decrease with increasing LNO wt.%. The electrical conductivity of LNO, LNO–LNF73, LNO–LNF55, LNO–LNF37 and LNF are 61.2–72.5, 95.1–106.9, 160.5–166.5, 290.9–298.8 and 503.9–526.6 S cm^{-1} between 500 and 700 °C, respectively. Clearly, LNO alone was not favorable for ideal SOFC cathode due to its low electrical conductivity. When adding a small amount of LNF (30 wt.%), LNO–LNF73 approached about 100 S cm^{-1} which met the criteria for electrical conductivity. The more LNF added in the composite cathode, the higher electrical conductivity was obtained. However, after the electrical conductivity of the cathode approached 100 S cm^{-1}, the oxygen ion conductivity will mainly affect the cathode performance. So apart from the electrical conductivity requirement, for proton-blocking composite cathode, the higher oxygen ion conductivity may be favorable for a better cathode performance and then further optimize the single cell performance. The Arrhenius curves of conductivities were plotted in Fig. 2(b). Linear relationships could
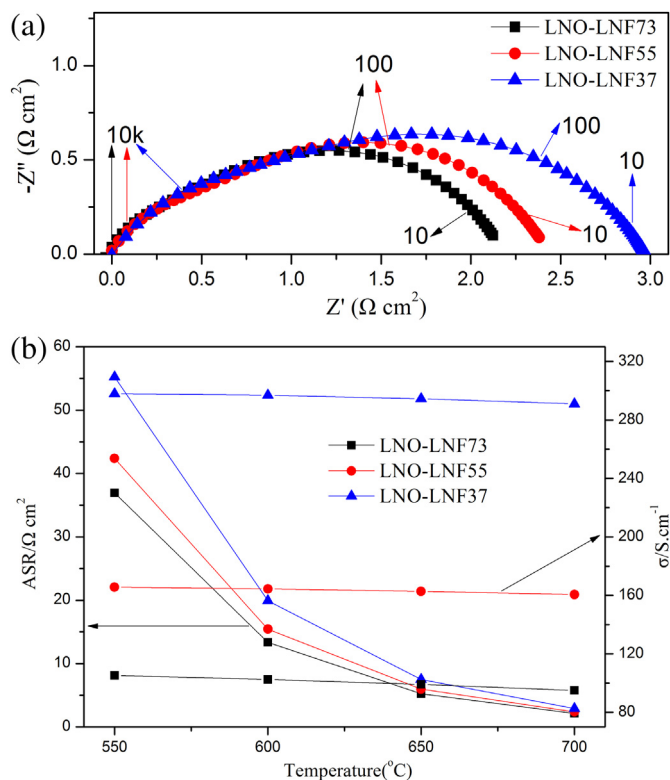
be observed at low temperature (200–550 °C) for LNO and among the testing temperature for others. The activity energy (Ea) was obtained according to $\sigma = (C/T) \exp(-E_a/kT)$, where k is Boltzmann constant and C is pre-exponential constant. The E_a of LNO, LNO–LNF73, LNO–LNF55, LNO–LNF37 and LNF are 0.052, 0.043, 0.067, 0.061 and 0.053 eV. Chen et al. [34] reported the electrical conductivity of LNO and the calculated E_a is 0.069 eV which is larger than this work. Yang et al. [43] also showed it that the E_a of $Pr_{1.2}Sr_{0.8}NiO_{4+\delta}$ is 0.034 eV, which is much less. Among the five different cathodes, LNO–LNF73 has the lowest activity energy which indicates that the cathode LNO–LNF73 is the most optimal combination. Therefore we may predict that LNO–LNF73 will have the best cell performance which contain the lowest polarizations and the highest power densities.

3.3. Characterization of symmetrical cells

Fig. 3(a) shows the typical electrochemical impedance spectra (EIS) in Nyquist plot of three symmetrical cells with cathode LNO–LNF73, LNO–LNF55, LNO–LNF37 based on BZCY electrolyte at 700 °C. In order to study different processes that happen at electrode, it is important to explain the different semicircles involved.

Fig. 3. (a) EIS of symmetric cells with different cathode at 700 °C, (b) the ASR comparison and the electrical conductivity of three different cathode from 550 to 700 °C.

Table 2
Results of the electrochemical impedance spectra for LNO–LNF73, LNO–LNF55 and LNO–LNF37 at 700 °C.

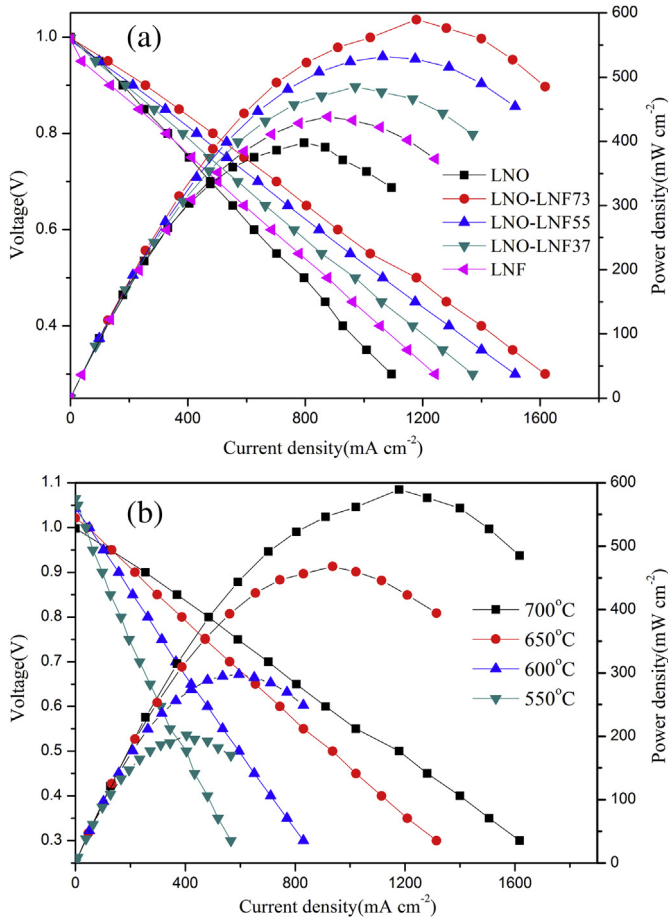| Electrode composition	R_H (Ω cm^2)	C_H (F cm^2)	f_H (Hz)	R_L (Ω cm^2)	C_L (F cm^2)	f_L (Hz)
LNO–LNF73	0.426	1.01×10^{-4}	3711	1.688	6.44×10^{-4}	146.5
LNO–LNF55	0.571	6.07×10^{-5}	4590	1.811	5.00×10^{-4}	175.8
LNO–LNF37	0.826	1.99×10^{-5}	9668	2.141	1.62×10^{-4}	459

Fig. 4. I–V and I–P curves of (a) single cells with different cathodes at 700 °C, (b) the single cell with LNO–LNF73 as cathode at 550–700 °C.

As can be seen from Fig. 3(a), the spectra measured with different cathodes were asymmetric in shape, implying more than one electrode process. The impedance spectra were fitted according to an $LR(R_HQ_H)(R_LQ_L)$ equivalent circuit model. The (RQ) components correspond to the involved electrode processes. For (RQ) components, R is the resistance and Q is the constant phase element. The impedance Z_Q of a constant phase element Q and equivalent capacitance C of the (RQ) components can be calculated according to the following equations [44]:

$$Z_Q = \frac{1}{Q(i \cdot \omega)^n} \quad (2)$$

$$C = \frac{(RQ)^{1/n}}{R} \quad (3)$$

where, ω is the angular frequency and n is an exponent. The constant phase element Q represents an ideal capacitor and an ideal

resistor when $n = 1$ and $n = 0$, respectively. When $0 < n < 1$, the circuit component reflects inhomogeneity of the electrode system. The relaxation frequency f of an electrode process corresponding to a specific (RQ) component can be calculated by the following equation [44]:

$$f = \frac{(RQ)^{-1/n}}{2\pi} \quad (4)$$

Table 2 lists the parameters of the circuit elements which are derived from Fig. 3(a). The equivalent capacitances and relaxation frequencies can be applied as characteristic parameters to identify the electrode processes. The electrode process corresponding to the component (R_HQ_H) had the equivalent capacitances of 10^{-5}–10^{-4} F cm^{-2} and the relaxation frequencies of 10^3–10^4 Hz with different cathodes. Thus, the electrode process is attributed to the charge transfer process of oxygen ions between the electrode and electrolyte [30,45]. The electrode processes corresponding to the component (R_LQ_L) showed the equivalent capacitances of 10^{-4} F cm^{-2} along with the relaxation frequencies of 10^2 Hz. Accordingly, the former process is assigned to the diffusion of atomic oxygen within the porous electrode followed by a charge transfer (surface oxygen exchange), while the latter is ascribed to the adsorption and dissociation of molecular oxygen on the surface of the electrode [30,46]. Obviously, only the contribution associated with polarization resistance (R_p) were shown, while the R_b corresponding to bulk resistance was omitted. And the polarization resistances of various electrode processes (R_H and R_L) presented an identical variation trend, both increasing with increasing the LNF (wt.%). The increase of R_H and R_L can be explained in terms of the gradually decreased oxygen-ion transport ability for less and less LNO. This result confirms that oxygen ions are more easily generated and transported in the electrode of LNO–LNF73, probably due to the high electrochemical activity for the oxygen reduction reaction and the high ionic conductivity in this electrode which is more favorable to the production and transportation of oxygen ions. When more LNF is added, the electrochemical activity for the oxygen reduction reaction is not so important, the gradually reduced LNO may affect the cathode more, for the ability to diffuse oxygen ions is more and more weak. So among the three symmetrical cells, LNO–LNF73|BZCY|LNO–LNF73 is capable of offer sufficient both electrochemical activity and oxygen-ions transportation rather than other compositions.

The area specific resistances (ASRs) and the electrical conductivity of three kind of electrodes in temperature range of 550–700 °C are shown in Fig. 3(b). One can be seen that, an obvious drop of ASR is observed for three cells with increasing temperature. More importantly, the more LNO in cathode, the invariably lower of the cell ASR at the same temperature which can be interpreted by the above discussion.

3.4. Electrochemical performance of single cells

To characterize the cathode performance of LNO–LNF, different button cells using NiO–BZCY as anode and BZCY as electrolyte were

Table 3

The OCVs and the MPDs of single cells with LNO, LNO–LNF73, LNO–LNF55, LNO–LNF37 and LNF as cathode measured from 550 to 700 °C.

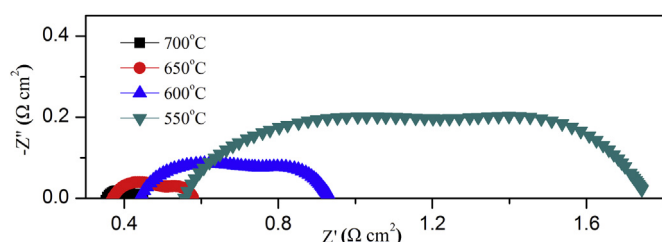| OCV(V) MPD (mW cm^{-2})	LNO		LNO–LNF73		LNO–LNF55		LNO–LNF37		LNF	
	OCV	MPD	OCV	MPD	OCV	MPD	OCV	MPD	OCV	MPD
700 °C	1	398	0.998	590	0.993	532	0.998	486	0.996	439
650 °C	1.023	283	1.021	469	1.021	403	1.023	393	1.02	362
600 °C	1.044	196	1.043	298	1.045	273	1.043	264	1.037	252
550 °C	1.063	120	1.065	203	1.067	175	1.064	160	1.052	149

Fig. 5. Electrochemical impedance spectra (EIS) of the single cell with LNO–LNF73 as cathode measured under open-circuit conditions from 500 to 700 °C.

Fig. 6. The maximum power densities and the polarization resistances of different single cells at 700 °C.

fabricated and measured under conventional conditions (humidified hydrogen as the fuel gas; static air as the oxidant). For comparison, single cells with single phase LNO and LNF cathodes were also fabricated. As all different single cells were fabricated in the same synthesis method, and has almost the identical thick BZCY electrolyte which is about 20 μm, so it can be considered that the discrepancy in electrochemical efficiency was caused by the different cathode used. The I−V and I−P curves of single cells with different cathodes at 700 °C are plotted in Fig. 4(a). The open-circuit voltages (OCVs) of single cells with LNO, LNO–LNF73, LNO–LNF55, LNO–LNF37 and LNF as cathode after anode reduction are 1, 0.998, 0.993, 0.998 and 0.996 V, corresponding to the maximum power densities (MPDs) that are 398, 590, 532, 486, 439 mW cm^{-2} at 700 °C, respectively. As it is shown, at the same voltage value, the single cell with LNO–LNF73 as cathode has the highest current density and this would lead to the highest power density, which validates by the MPD values. The single cell with LNO–LNF73 as cathode show the highest power output reaching 203, 298, 469 and 590 mW cm^{-2} at 550, 600, 650 and 700 °C which is plotted in Fig. 4(b). The OCVs and the MPDs of different single cells with composite cathodes contain are all shown in Table 3. The OCV values confirm that the electrolyte membranes in different single cells are sufficiently dense to resist gas leakage. The highest power output of the one with LNO–LNF73 as cathode demonstrates that LNO–LNF73 possesses the best electrochemical properties and corroborates the results of the impedance measurement discussed later.

Typical electrochemical impedance spectra (EIS) at 550−700 °C with the cathode LNO–LNF73 were obtained under open-circuit conditions, as shown in Fig. 5. In the EIS plots, the high-frequency intercept corresponds to the ohmic resistance (R_o) of the cell, including the ionic resistance of the electrolyte, the electronic resistance of the electrodes and some contact resistance associated with the interfaces of the components. The low-frequency intercept corresponds to the total resistance (R_t) of the cell. The difference between the two intercept indicates the interfacial polarization resistance (R_p) of the cell. The EIS at 550−700 °C with other cathodes were not put here for the similar trend. And the R_o and R_p of different single cells range of 550−700 °C are all shown in Table 4. As can be seen from Table 4, all resistances decrease with increasing temperature, indicating that the corresponding electrochemical reactions are thermally activated processes. In the case of the cell
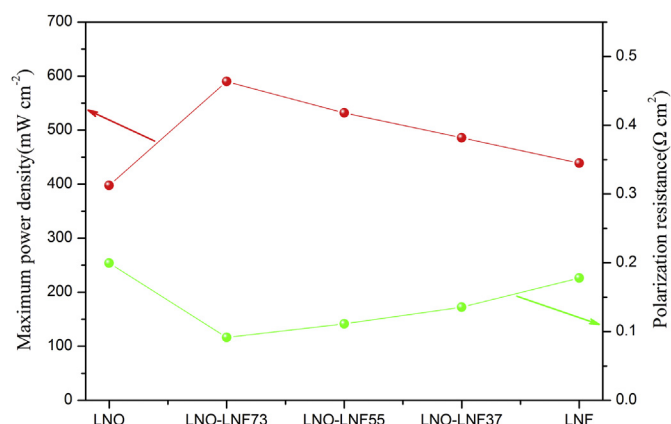
with LNO–LNF73 as cathode, the value of R_p decrease from 1.187 to 0.091 Ω cm^2 with increasing temperature from 550 to 700 °C. However, the value of R_o only decreases from 0.557 to 0.357 Ω cm^2 under the same conditions. It is easy to see that the cell R_p governs the downward trend of R_t and plays a major role in determining the total resistance of the cell below 600 °C. So the purpose of developing better cathode materials is to reduce R_p and to optimize cell performance, which thus ultimately realizes low-temperature cell operation. In these five different cathodes, LNO–LNF73 has the lowest R_p that are 0.091, 0.206, 0.486 and 1.187 Ω cm^2 at 700, 650, 600 and 550 °C, which is consistent with the highest power output discussed before.

To further analyze the electrochemical parameters, the MPDs and the R_p of single cells with different cathodes at 700 °C are shown in Fig. 6. It is clear that the single cell with single phase LNO as cathode generates the lowest power output. However, when adding a small amount of LNF (30 wt.%), the single cell with LNO–LNF73 as cathode shows the highest power output. But after continuing to add more LNF, single cells with LNO–LNF55 and LNO–LNF37 display decreased lower power output than that for the LNO–LNF73 cathode cell. Nevertheless, the composite cathodes contains LNO–LNF73, LNO–LNF55 and LNO–LNF37 reveal higher power outputs than the single phase cathode LNO or LNF. Meanwhile, the R_p indicates the contrary trends. The single cell with LNO has highest R_p, while the single cell with LNO–LNF73 has the lowest R_p. The MPDs and the R_p of single cells with different cathodes at 550, 600, 650 °C show a similar trend with those at 700 °C and the detailed plots are not put here. These results accord with the prediction proposed in the electrical conductivity analysis. So the electrochemical performance of the SOFC examined in this study indicates that LNO–LNF73 possesses best electrochemical properties among the five cathode materials and it is suitable as a cathode material for H-SOFCs.

Based on the very high electrochemical performance of LNO–LNF73, the cell performance is largely improved as compared to

Table 4
R_o and R_p of single cells with LNO, LNO–LNF73, LNO–LNF55, LNO–LNF37 and LNF as cathode measured from 550 to 700 °C.

| R_o and R_p (Ω cm^2)	LNO		LNO–LNF73		LNO–LNF55		LNO–LNF37		LNF	
	R_o	R_p	R_o	R_p	R_o	R_p	R_o	R_p	R_o	R_p
700 °C	0.420	0.199	0.357	0.091	0.321	0.111	0.355	0.135	0.306	0.178
650 °C	0.501	0.433	0.372	0.206	0.380	0.239	0.437	0.258	0.348	0.276
600 °C	0.641	0.962	0.445	0.486	0.498	0.505	0.533	0.570	0.413	0.616
550 °C	0.816	2.269	0.557	1.187	0.660	1.309	0.689	1.372	0.510	1.452

Table 5
Summary of the electrolyte film thickness (μm), cathode material, maximum power density (MPD, mW cm^{-2}) and interfacial polarization resistances (R_p, Ω cm^2) of the cells with BZCY-based electrolyte reported in literature.

| Electrolyte	Thickness	Cathode	MPD (700 °C)	R_p (Ω cm^2)	Ref.
$BaZr_{0.1}Ce_{0.7}Y_{0.2}O_{3-\delta}$	15 μm	$Ba_{0.5}Sr_{0.5}Zn_{0.2}Fe_{0.8}O_{3-\delta}$	486	0.1	[48]
$BaZr_{0.1}Ce_{0.7}Y_{0.2}O_{3-\delta}$	20 μm	$Ba_{0.5}Sr_{0.5}FeO_{3-\delta}-SDC$	696	0.044	[47]
$BaZr_{0.1}Ce_{0.7}Y_{0.2}O_{3-\delta}$	15 μm	$La_{0.5}Sr_{0.5}FeO_{3-\delta}-SDC$	449	0.11	[6]
$BaZr_{0.1}Ce_{0.7}Y_{0.2}O_{3-\delta}$	15 μm	$Ba_{0.85}La_{0.05}FeO_{3-\delta}-BZCY$	325	0.17	[16]
$BaZr_{0.1}Ce_{0.7}Y_{0.2}O_{3-\delta}$	20 μm	$Sm_{0.5}Sr_{0.5}FeO_{3-\delta}-BZCY$	341	0.1	[24]
$BaZr_{0.1}Ce_{0.7}Y_{0.2}O_{3-\delta}$	20 μm	$GaBaFeNiO_{5+\delta}$	456	0.15	[49]
$BaZr_{0.1}Ce_{0.7}Y_{0.2}O_{3-\delta}$	20 μm	$La_{0.6}Sr_{0.4}Fe_{0.9}Ni_{0.1}O_{3-\delta}$	405	0.14	[50]
$BaZr_{0.1}Ce_{0.7}Y_{0.2}O_{3-\delta}$	20 μm	LNO−LNF73	590	0.091	This work

those BZCY-based cells with cobalt-free cathodes reported in literature, as shown in Table 5. Evidently, the single cell with LNO−LNF73 as cathode shows higher MPD and lower R_p than most cobalt-free cathodes, indicating the superior of LNO−LNF73 among the cathodes. Although Sun et al. [47] reported a 20 μm thick BZCY-based single cell with $Ba_{0.5}Sr_{0.5}FeO_{3-\delta}-SDC$ as cathode whose MPD and R_p were 696 mW cm^{-2} and 0.044 Ω cm^2 at 700 °C, respectively. The MPD and the R_p are preferably better than this work which may be ascribed to the lower ohmic resistance (R_o = 0.31 Ω cm^2) and the better anode microstructure. Moreover, the cathode $Ba_{0.5}Sr_{0.5}FeO_{3-\delta}-SDC$ contains alkaline earth element barium and strontium as the main component, which potentially has the problem for chemical stability. In contrast, LNO−LNF73 could be more stable for alkaline earth free composition. The stability of the single cell with LNO−LNF73 as cathode based on BZCY electrolyte was evaluated under fuel cell testing conditions. As shown in Fig. 7, the OCV of the cell at 700 °C was recorded as a function of operation time with hydrogen (3% H$_2$O) as the fuel. The OCV kept stable after 70 h which indicates that the structure of the single cell was not broken after operating 70 h under open circuit condition. Due to the intrinsic advantages of LNO−LNF73, the cathode LNO−LNF73 could be considered as one of the best cobalt-free cathodes and we can conclude that LNO−LNF73 is a very promising cathode for H-SOFCs.

The microstructures of the cells were observed by SEM. Shown in Fig. 8 are the SEM images of the cross-sectional morphology of single cells with all cathodes contain. As can be seen, all cathodes have a good adherence with the BZCY electrolyte, and it has no interfacial reaction between the cathodes and the electrolyte. The fact also illustrates it that the cathode firing temperature used 1000 °C is appropriate. Fig. 9 shows cross-sectional views of single

cells with different cathodes, such as LNO, LNO−LNF73, LNO−LNF55, LNO−LNF37, LNF after testing and LNO−LNF73 before testing. Each SEM images contain a magnification cathode microstructure. As shown in Fig. 9, in all single cells, there are two porous electrodes, anode and cathode, well adhered on both side of dense BZCY electrolyte without any sign of cracking and delamination, suggesting a good thermal matching between parts. And the cathode microstructures are extremely similar. The thickness of the electrolyte in all single cells is about 20 μm. With nearly the same thick electrolyte as well as very close cathode microstructure, the different single cell performance should be owning to the intrinsic properties of different cathode. However, there are some large pores, nearly about 7 μm in size, which mainly resulted from the combustion of the pore-creating materials (such as starch in this work), existed at the anode electrolyte interface. The not optimized interfacial morphology not only decreased the active sites but also
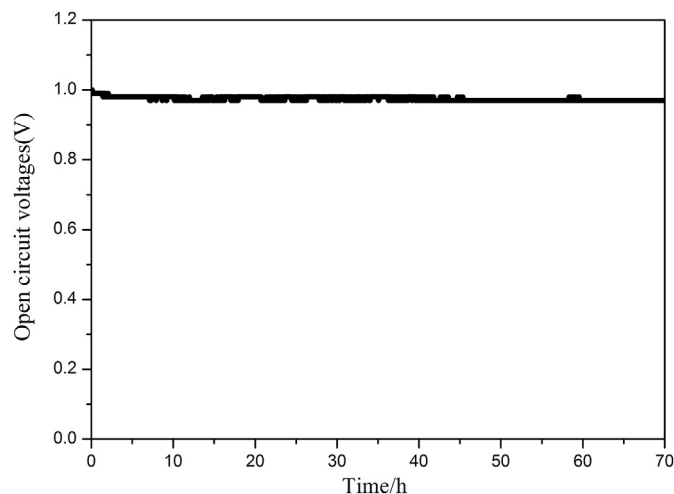
Fig. 7. The OCV of the single cell with LNO−LNF73 as cathode based on BZCY electrolyte at 700 °C as a function of time with hydrogen (3% H$_2$O) as the fuel.
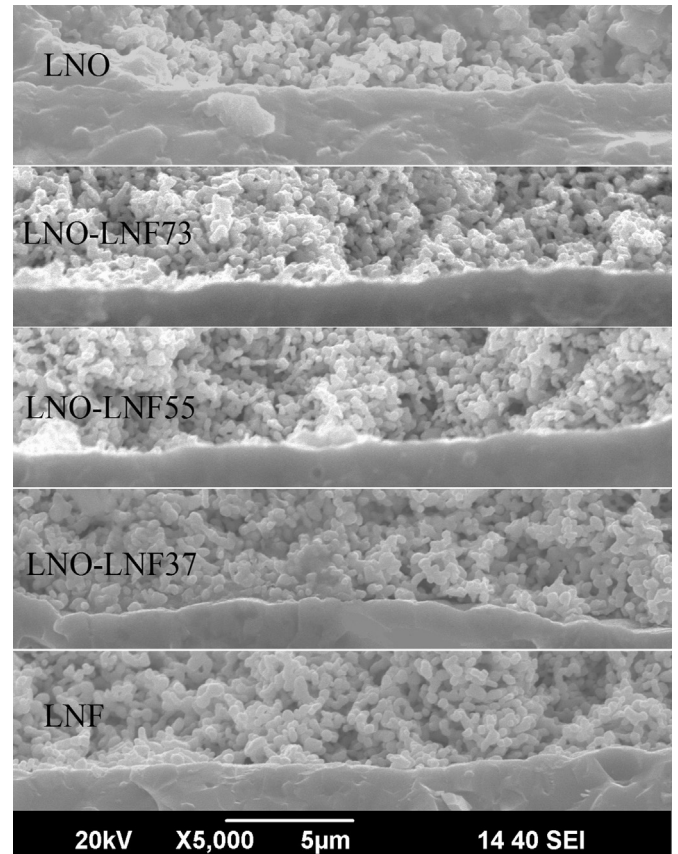
Fig. 8. Merged SEM images of the cross-sectional morphology of single cells with all cathodes contain.
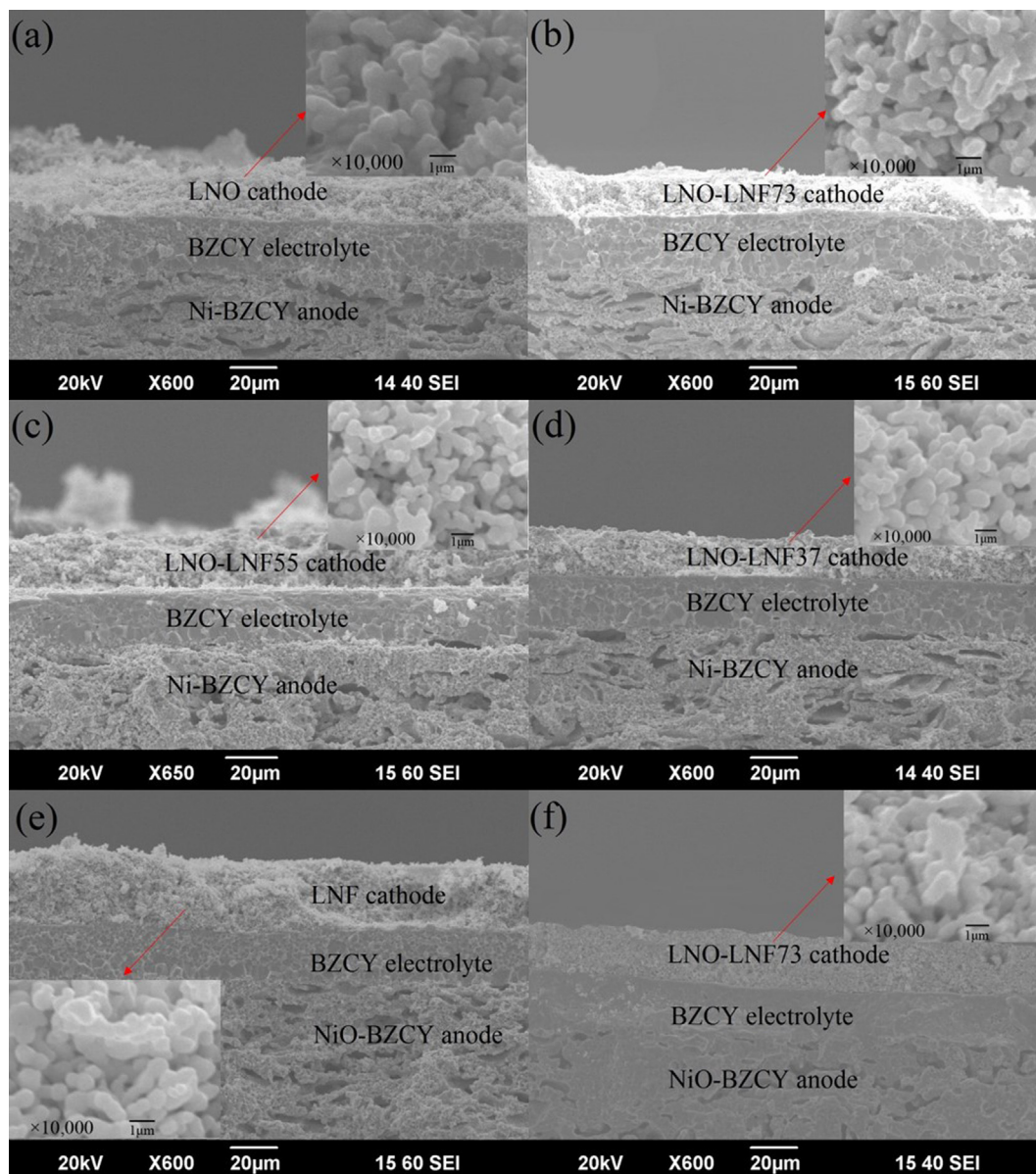
Fig. 9. Cross-section SEM images of single cell with cathode (a) LNO, (b) LNO–LNF73, (c) LNO–LNF55, (c) LNO–LNF37, (e) LNF after testing and (f) LNO–LNF73 before testing.

increased the contact resistance. Whatever, the electrochemical performance of the cell can be further improved if the microstructures of the anode and anode–electrolyte interface are appropriately tailored and optimized.

4. Conclusions

Cobalt-free proton-blocking LNO–LNF composites were evaluated as cathodes for BZCY-based H-SOFC. A good chemical compatibility between the two constituent phases below 1100 °C has been ascertained using XRD. The electrical conduction study reveals that LNO–LNF73 meets sufficient electrical conductivity (95.1–106.9 S cm^{-1} from 500 to 700 °C) and is favorable to cathode using for the most optimized combination of oxygen ion conductivity and electrical conductivity among all composite cathodes. It was found that after introducing LNF composition into LNO cathode, the single cell showed higher MPDs and lower R_p than single phase cathode LNO and LNF. Meanwhile, the cathode LNO–LNF73

showed the highest power output reaching 590 mW cm^{-2} and the lowest R_p that was 0.091 Ω cm^2 at 700 °C. The electrochemical performance is one of the best ever reported, which is comparable to those observed for other cobalt-free cathodes and even better. It is concluded that the LNO–LNF73 composite cathode is a promising high performance cathode material for H-SOFCs.

References

[1] Z. Ding, Z. Yang, D. Zhao, X. Deng, G. Ma, J. Alloys Compd. 550 (2013) 204–208.
[2] L. Bi, E. Fabbri, Z. Sun, E. Traversa, Solid State Ionics 196 (2011) 59–64.

[3] E. Fabbri, A. Depifanio, E. Dibartolomeo, S. Licoccia, E. Traversa, Solid State Ionics 179 (2008) 558—564.
[4] Z. Shao, S.M. Haile, Nature 431 (2004) 170—173.
[5] Z. Wang, M. Liu, W. Sun, D. Ding, Z. Lü, M. Liu, Electrochem. Commun. 27 (2013) 19—21.
[6] W. Sun, Z. Zhu, Y. Jiang, Z. Shi, L. Yan, W. Liu, Int. J. Hydrogen Energy 36 (2011) 9956—9966.
[7] E. Fabbri, I. Markus, L. Bi, D. Pergolesi, E. Traversa, Solid State Ionics 202 (2011) 30—35.
[8] F. Zhao, Q. Liu, S. Wang, K. Brinkman, F. Chen, Int. J. Hydrogen Energy 35 (2010) 4258—4263.
[9] X.-Z. Fu, J.-L. Luo, A.R. Sanger, N. Luo, K.T. Chuang, J. Power Sources 195 (2010) 2659—2663.
[10] K.D. Kreuer, Annu. Rev. Mater. Res. 33 (2003) 333—359.
[11] W. Sun, S. Fang, L. Yan, W. Liu, J. Electrochem. Soc. 158 (2011) B1432.
[12] C. Zuo, S. Zha, M. Liu, M. Hatano, M. Uchiyama, Adv. Mater. 18 (2006) 3318—3320.
[13] F. Zhao, S. Wang, K. Brinkman, F. Chen, J. Power Sources 195 (2010) 5468—5473.
[14] W. Sun, L. Yan, B. Lin, S. Zhang, W. Liu, J. Power Sources 195 (2010) 3155—3158.
[15] Y. Lin, R. Ran, Z. Shao, Int. J. Hydrogen Energy 35 (2010) 8281—8288.
[16] L. Yan, H. Ding, Z. Zhu, X. Xue, J. Power Sources 196 (2011) 9352—9355.
[17] L. Yang, C. Zuo, S. Wang, Z. Cheng, M. Liu, Adv. Mater. 20 (2008) 3280—3283.
[18] B. Lin, H. Ding, Y. Dong, S. Wang, X. Zhang, D. Fang, G. Meng, J. Power Sources 186 (2009) 58—61.
[19] L. Yang, Z. Liu, S. Wang, Y. Choi, C. Zuo, M. Liu, J. Power Sources 195 (2010) 471—474.
[20] K. Xie, R. Yan, D. Dong, S. Wang, X. Chen, T. Jiang, B. Lin, M. Wei, X. Liu, G. Meng, J. Power Sources 179 (2008) 576—583.
[21] L. Zhang, W. Yang, Int. J. Hydrogen Energy 37 (2012) 8635—8640.
[22] Z. Zhu, Z. Tao, L. Bi, W. Liu, Mater. Res. Bull. 45 (2010) 1771—1774.
[23] K. Zhang, L. Ge, R. Ran, Z. Shao, S. Liu, Acta Mater. 56 (2008) 4876—4889.
[24] X. Lu, Y. Chen, Y. Ding, B. Lin, Int. J. Hydrogen Energy 37 (2012) 8630—8634.
[25] R. Sayers, M. Rieu, P. Lenormand, F. Ansart, J.A. Kilner, S.J. Skinner, Solid State Ionics 192 (2011) 531—534.
[26] M.J. Escudero, A. Fuerte, L. Daza, J. Power Sources 196 (2011) 7245—7250.
[27] F. Mauvy, C.c. Lalanne, J.-M. Bassat, J.-C. Grenier, H. Zhao, L. Huo, P. Stevens, J. Electrochem. Soc. 153 (2006) A1547.
[28] C. Laberty, F. Zhao, K.E. Swider-Lyons, A.V. Virkar, Electrochem. Solid State Lett. 10 (2007) B170.
[29] A.M. Hernández, L. Mogni, A. Caneiro, Int. J. Hydrogen Energy 35 (2010) 6031—6036.
[30] K. Zhao, Q. Xu, D.-P. Huang, M. Chen, B.-H. Kim, J. Solid State Electrochem. 16 (2012) 2797—2804.
[31] Y. Shen, H. Zhao, K. Świerczek, Z. Du, Z. Xie, J. Power Sources 240 (2013) 759—765.
[32] J. Rodriguezcarvajal, M.T. Fernandezdiaz, J.L. Martinez, J. Phys. Condens. Matter 3 (1991) 3215—3234.
[33] Y. Shen, H. Zhao, X. Liu, N. Xu, Phys. Chem. Chem. Phys. 12 (2010) 15124—15131.
[34] M. Chen, B.H. Moon, S.H. Kim, B.H. Kim, Q. Xu, B.G. Ahn, Fuel Cells 12 (2012) 86—96.
[35] S.P. Simner, J.F. Bonnett, N.L. Canfield, K.D. Meinhardt, V.L. Sprenkle, J.W. Stevenson, Electrochem. Solid State Lett. 5 (2002) A173.
[36] R. Chiba, F. Yoshimura, Y. Sakurai, Solid State Ionics 124 (1999) 281—288.
[37] B. Huang, X.-j. Zhu, Y. Lv, H. Liu, J. Power Sources 209 (2012) 209—219.
[38] R. Peng, T. Wu, W. Liu, X. Liu, G. Meng, J. Mater. Chem. 20 (2010) 6218.
[39] W. Sun, L. Yan, Z. Shi, Z. Zhu, W. Liu, J. Power Sources 195 (2010) 4727—4730.
[40] D.S. McLachlan, M. Blaszkiewicz, R.E. Newnham, J. Am. Ceram. Soc. 73 (1990) 2187—2203.
[41] Z. Zhu, L. Yan, W. Sun, H. Liu, T. Liu, W. Liu, J. Power Sources 217 (2012) 431—436.
[42] V.V. Kharton, A.P. Viskup, E.N. Naumovich, F.M.B. Marques, J. Mater. Chem. 9 (1999) 2623—2629.
[43] J. Yang, J. Cheng, Q. Jiang, Y. Wang, R. Wang, J. Gao, Int. J. Hydrogen Energy 37 (2012) 1746—1751.
[44] D. Chen, R. Ran, K. Zhang, J. Wang, Z. Shao, J. Power Sources 188 (2009) 96—105.
[45] M.J. Escudero, A. Aguadero, J.A. Alonso, L. Daza, J. Electroanal. Chem. 611 (2007) 107—116.
[46] K. Zhao, Q. Xu, D.-P. Huang, M. Chen, B.-H. Kim, Ionics 18 (2011) 75—83.
[47] W. Sun, Z. Shi, S. Fang, L. Yan, Z. Zhu, W. Liu, Int. J. Hydrogen Energy 35 (2010) 7925—7929.
[48] H. Ding, B. Lin, X. Liu, G. Meng, Electrochem. Commun. 10 (2008) 1388—1391.
[49] Z. Yang, Z. Ding, J. Xiao, H. Zhang, G. Ma, Z. Zhou, J. Power Sources 220 (2012) 15—19.
[50] F. Zhang, Z. Yang, H. Wang, W. Wang, G. Ma, Fuel Cells 12 (2012) 749—753.